Urban development induced subsidence in deltaic environments: A case study in Hanoi, Vietnam

Luke Bateson [a,*], Alessandro Novellino [a], Ekbal Hussain [a], Raushan Arnhardt [a], Ho Khanh Nguyen [b]

[a] *British Geological Survey, Nicker Hill, Keyworth, Nottingham NG12 5GG, United Kingdom*
[b] *Center for Information, Archives and Museum of Geology (CIAMG) - Vietnam Geological Department (VGD), Hanoi, Viet Nam*

ABSTRACT

Hanoi has experienced rapid urbanisation over the last few decades, putting intense pressure on its natural resources, such as groundwater, but also on the local authorities to meet demand for infrastructure, housing and public amenities. Recent studies using Interferometric Synthetic Aperture Radar (InSAR) measured rates of subsidence in Hanoi documenting the evolution of the subsiding areas. These studies have primally attributed the high rates of subsidence to the increased extraction of groundwater. In this study we use Sentinel 1 InSAR data for six years between July 2015 and January 2021 to examine subsidence patterns across Hanoi and link them to the development of urban areas. We find that although groundwater extraction undoubtedly plays a significant role, there is a clear spatial and temporal link between new development and the areas of subsidence. The use of historical optical satellite imagery allows the evolution of the development to be linked to the InSAR ground motion time series. A correlation exists between subsidence and the reclamation of agricultural land, often flooded rice fields, for building via the dumping of aggregate to create dry, raised areas on which to build. We illustrate our findings with examples where newly developed areas are co-incident with areas of subsidence, we show the relationships between the stages of the ground loading and the rate of the resulting subsidence. Ultimately, we extract rates of motion for each year following ground loading. The collected rates of subsidence for over 40 locations of new development allows us to determine the rates of subsidence due to the consolidation process. This relationship enables an understanding of subsidence rate with time which has clear applications in the planning of future developments on thick superficial geological deposits.

1. Introduction

The world is increasingly becoming urbanised, in 2018 55 per cent of the world's population lived in urban areas and by 2050 this is projected to be 68 per cent. Currently North America, Latin America and Europe represent the most urbanised regions (82, 81 and 74 per cent respectively) whilst Africa and Asia are the most rapidly urbanising areas (United Nations, Department of Economic and Social Affairs, Population Division, 2019). Increased urbanisation leads to pressures on the environment which in turn can lead to an increase in urban geohazards, one such hazard is subsidence. Natural subsidence due to compaction of sediment under its own weight is enhanced by anthropogenic effects such as groundwater withdrawal (Boni et al., 2016), reclamation of land (Tosi et al., 2013), underground (Strozzi et al., 2011) and above ground construction and mining (Gee et al., 2020). Many of these subsidence

mechanisms are prevalent in geological settings with thick sequences of recent sediments, such as coastal lowlands, deltas and river plains. With eight of the ten world's most rapidly developing cities (United Nations, Department of Economic and Social Affairs, Population Division, 2019) in such geological settings the impacts of ground subsidence are expected to increase in the future. There is therefore a need for subsidence mechanisms, and rates, to be better understood and quantified to allow responsible authorities to plan for such geohazards as urban areas expand.

Hanoi city is the capital and second largest city of Vietnam with 7.4 million inhabitants (GSOVa, 2019; GSOVb, 2019). As a result of rapid urbanisation causing pressures on resources and the environment, the government of Vietnam officially presented the Hanoi Master Plan (HMP) in July 2011. The target of the master plan is to develop Hanoi as a sustainable and resilient city by 2030 with a vision to establish the city

---

as one of the most liveable, sustainable, and attractive world capital cities by 2050. To achieve this objective, planners have identified sites for urban expansion in satellite cities outside of the current city limits (Institute and of Architecture, Urban and Rural Planning (VIAP), 2011). The HMP has resulted in the development of rural areas around Hanoi, two such areas are Ha Dong and Hoai Duc (Fig. 1).

Groundwater plays an important role for the economic and social health of populations worldwide, especially in urban centres. Cities need to supply water in various combinations as per demands of their private, public, industrial and commercial users. The urbanisation process has always altered the quality and quantity of the local aquifer systems in various ways (Wakode et al., 2018). Groundwater extraction in Hanoi has long been recognised as the principal water source for the city and the negative effects of rapid urban growth on the groundwater system have been identified early (Trafford et al., 1996). In more recent years, several studies of ground motion using Interferometric Synthetic Aperture Radar (InSAR) have measured rates of subsidence in Hanoi and, via the use of successive satellite sensors have documented the evolution of the subsiding areas (Le et al., 2016; Bui et al., 2021). Such InSAR studies invariably link the subsidence observed in Hanoi to groundwater abstraction and the authors have used these relationships to parameterise subsidence models, which have been used to forecast subsidence in Hanoi over the coming decades (Nguyen et al., 2022).

Although some studies recognise the spatial link between new development areas and subsidence (Dang et al., 2014), the link is made to the increased extraction of groundwater to support these new residential areas and the impact of that on the pore water pressure within unconsolidated sediments with high porosity. New building complexes within Hanoi are founded on deep piled foundations, in the majority of cases this means that these buildings are stable. However, differential motion between the building (founded on piles) and the surrounding ground has been documented (Peduto et al., 2017; Dang et al., 2014), proving differential subsidence does occur. Since the buildings are stable and groundwater is routinely extracted the groundwater is cited as the primary mechanism for the observed subsidence.

In this paper we propose that a significant role in the subsidence observed between 2015 and 2021 is due to the anthropogenic compaction of the unconsolidated Holocene sediments. Although groundwater extraction has been proven to play an important role in some of the areas of InSAR-observed subsidence (Bui et al., 2021), we will demonstrate that ground deformation is also driven by new urban development, specifically when previously wet land is loaded with aggregate to create dry, raised areas on which the new buildings are developed. To illustrate our case, we show examples where newly developed areas are co-incident, in space and time, with areas of subsidence, we show the temporal relationships between the stages of the ground loading and the rate of the subsidence. We extract yearly rates of motion for the years following ground loading and do so for many locations to understand how the rate declines as the consolidation process occurs. This enables the derivation of a general trend of subsidence rate with time due to just the consolidation process, which might have applications in the planning of urban expansion in the many growing cities sited on thick superficial geological deposits.

2. Study site and geological setting

The Hanoi Metropolitan Area is a ~3343 km^2 area located in the northern part of Vietnam, within the Red River delta plain and nearly 90 km from the coastline (Fig. 1). It encompasses Hanoi city, and is the commercial, cultural and educational centre of Northern Vietnam (Vu and Nghiem, 2016). A recent study on land cover changes in Hanoi highlighted that between 1975 and 2020 artificial surfaces have
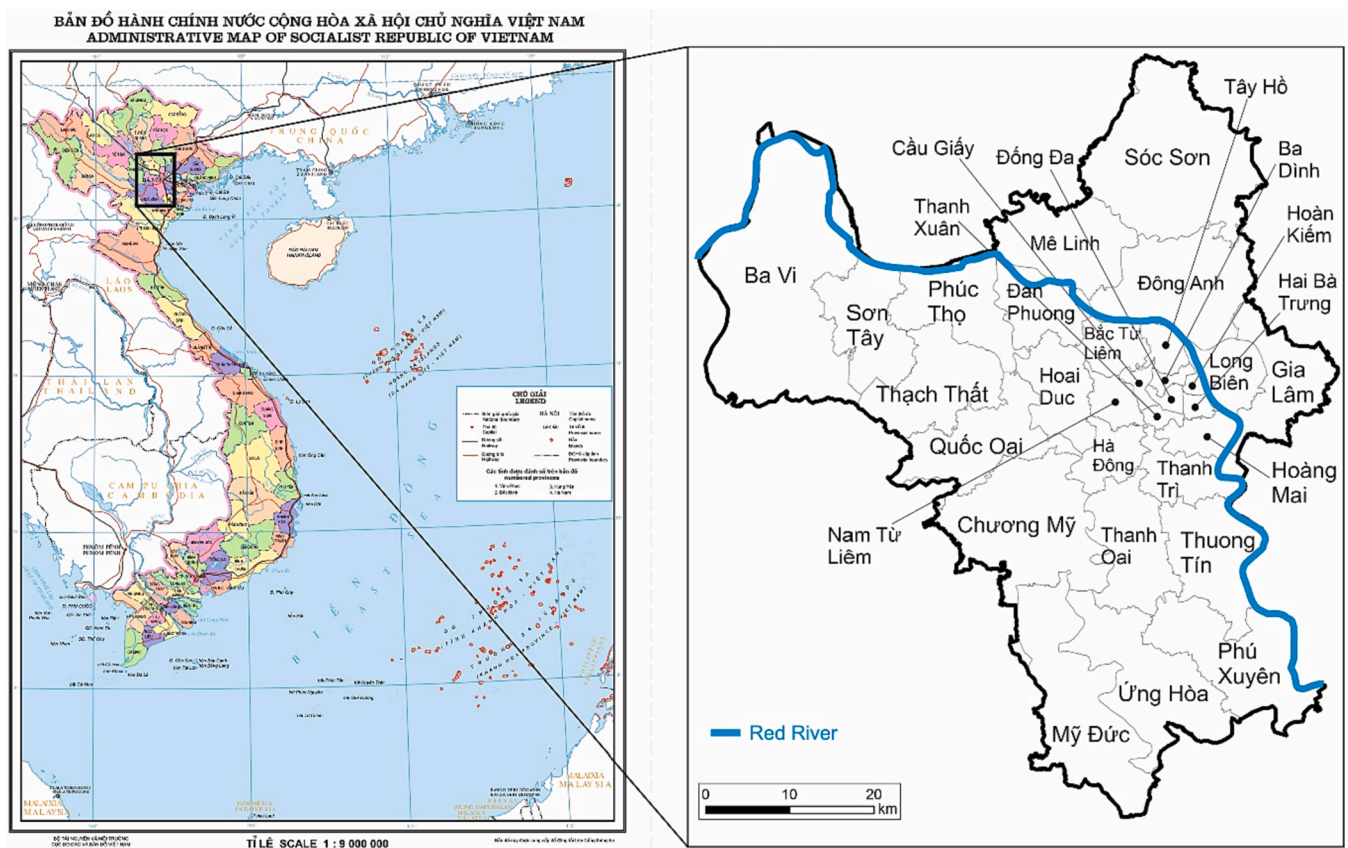

Fig. 1. Location map of the Hanoi *Metropolitan Area* as black polygon (left, © intellectual property office of Vietnam) and the main administrative boundaries of the 30 districts within the Hanoi *Metropolitan Area (Administrative outlines © OpenStreetMap contributors and the GIS user community)*. Coordinate system: WGS1984.

increased by 15.5 % while forests have decreased by 26.7 %. (Novellino et al., 2021). In the HMP, the population of Hanoi is projected to reach 9–9.2 million by 2030 and approximately 10.8 million by 2050 (Kubota et al., 2017, Liou et al., 2021). To address potential issues related to social, economic, physical, and environmental aspects, the HMP proposes a series of spatial development strategies for the city which consider the high subsidence susceptibility for the area (Herrera-García et al., 2021).

Located within the Red River Delta, the geology of Hanoi consists of unconsolidated Quaternary sediments of fluvial and marine origin scattered over a flat basin of 11,000 km^2 and prone to subsidence (Dang et al., 2014). Lying on top of Neogene shallow marine deposits (Trafford et al., 1996), the Quaternary sediments are divided into 24 layers (Table 1), at the top is the Thai Bihn formation composed of sand and clay of recent alluvial origin. At the base of the Quaternary is the Le Chi formation, which is generally coarser grained being composed of sand, gravel, cobbles, and pebbles but also of alluvial origin. (Phi and Strokova, 2015). Total thickness of the Quaternary deposits range between 50 m and 90 m. To understand the spatial distribution of these deposits within the Hanoi Metropolitan Area, 271 boreholes (Fig. 2a) were used to create cross sections and a 3D geological model for central Hanoi using GoCad geological modelling software (Fig. 2b; Arnhardt et al.,

Table 1
Geology of Hanoi detailing the composition of the 24 layers within the Quaternary.

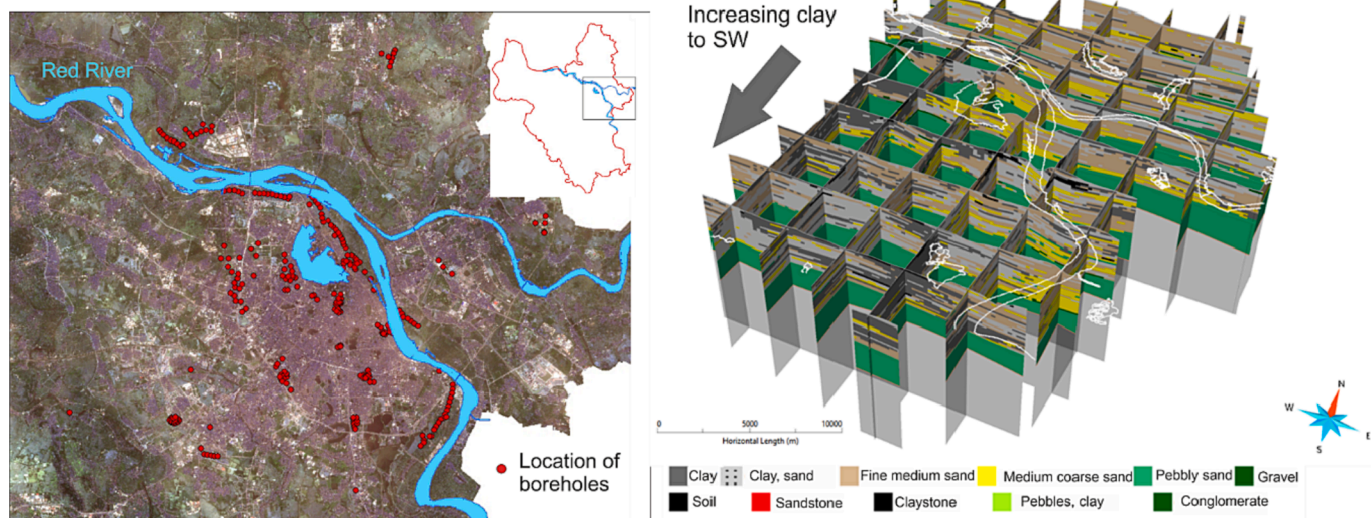| System	Division	Formation	Thickness (m)	Lithology	UAS/LAS	Hydrogeological significance	Layer	Lithology
Quaternary	Holocene	Thai Binh	11–46	Recent alluvial sediment (sand, clay sand, sandy clay)	Upper aquifer System	Unconfined aquifer	Layer 2	Very soft sandy clay with organic matters (bottom sediments of lakes and ponds)
							Layer 3	Brown and pinkish-brown firm sandy clay, interstratified with clayey sand
							Layer 4	Saturated brownish-grey fine-grained and loose sand, some places with gravel
							Layer 5	Yellowish-grey stiff to firm clay
							Layer 6	Yellowish grey and brown stiff to firm sandy clay
							Layer 7	Saturated brownish-grey very soft to soft sandy clay with organic matters
							Layer 8	Brownish grey firm sandy clay, interstratified with clayey sand and sand
							Layer 9	Saturated greenish-grey fine-grained medium dense sand
							Layer 10	Brownish grey firm sandy clay, interstratified with clayey sand and sand
		Hai Hung	5–17	Lacustrine sediment (clay)		Aquitard not always present	Layer 11	Saturated dark grey very soft to soft sandy clay with organic matters
							Layer 12	Green grey stiff to firm clay
							Layer 13	Dark grey very soft sandy clay with organic matters
	Pleictocene	Vinh Phuc	5–18	Lacustrine sediments (clay, sandy clay)		Aquitard not always present	Layer 14	Light grey and yellowish-grey stiff clay
							Layer 15	Multi-coloured (brown, yellow, red) very stiff to stiff sandy clay
							Layer 16	Dark grey very soft to soft sandy clay with organic matters
							Layer 17	Yellowish-grey plastic clayey sand, interstratified with sandy clay or sand
							Layer 18	Saturated brown and yellowish-brown fine-grained medium dense to dense sand
							Layer 19	Saturated yellowish-grey and light grey medium and coarse-grained dense to very dense sand, some places with gravel and pebbles
		Ha Noi	21	Alluvial deposits (clay)	Lower Aquifer System	Aquitard	Layer 20	Brownish grey firm sandy clay, some places with organic matters
							Layer 21	Grey plastic clayey sand, some places with gravel
							Layer 22	Saturated gravel and pebbles, some places with grey and yellowish-grey very dense coarse-grained sand
		Le Chi	28	Alluvial deposits (sand, gravel, cobbles, pebbles)		Mainly confined aquifer	Layer 23	Grey and brown plastic clayey sand, some places with gravel;
							Layer 24	Saturated gravel and pebbles, fine-grained and coarse-grained brownish-grey and yellowish-grey very dense sand with sandy clay
Tertiary	Pliocene	Vinh Bao	150	Estuarine to shallow marine formation (cobbles and pebbles, sandstone, siltstone, shale)		Aquifer		

Fig. 2. A. (left) location of boreholes in central hanoi used to create a 3d geological model, b. (right). Cross sections of the resulting 3d geological model showing increasing clay towards the south west. "World Imagery". Copyright © Esri. All rights reserved.

2023).

3. Datasets and methodology

The interpretation of the ground motion has been conducted by firstly processing the Sentinel-1 satellite data (Section 3.1) and then using Machine Learning techniques to exploit the results with a combination of Principal Component Analysis (PCA) and cluster analysis (Section 3.2).

3.1. InSAR processing

We downloaded 147 Sentinel-1A Single Look Complex images over

the Hanoi city region (Longitude, Latitude: 105.82, 21.02) from the Alaska Satellite Facility. These images are from descending track 91 spanning the dates 2 July 2015 to 7 January 2021 and have a return period of 12 days. We performed initial InSAR processing by making interferograms with every 2 consecutive pairs of SLC images using the Interferometric synthetic aperture radar Scientific Computing Environment (ISCE) software (Rosen et al., 2012, 2021), which resulted in 291 interferograms. Two consecutive small baseline interferograms allows us to build a redundant network of interferograms so that we can check for unwrapping errors using phase closure techniques. To improve the signal-to-noise ratio we multi-looked each interferogram by 3 pixels in azimuth and 9 pixels in range giving ground pixel sizes of approximately 50 m. Phase unwrapping was based on SNAPHU (Statistical-cost,
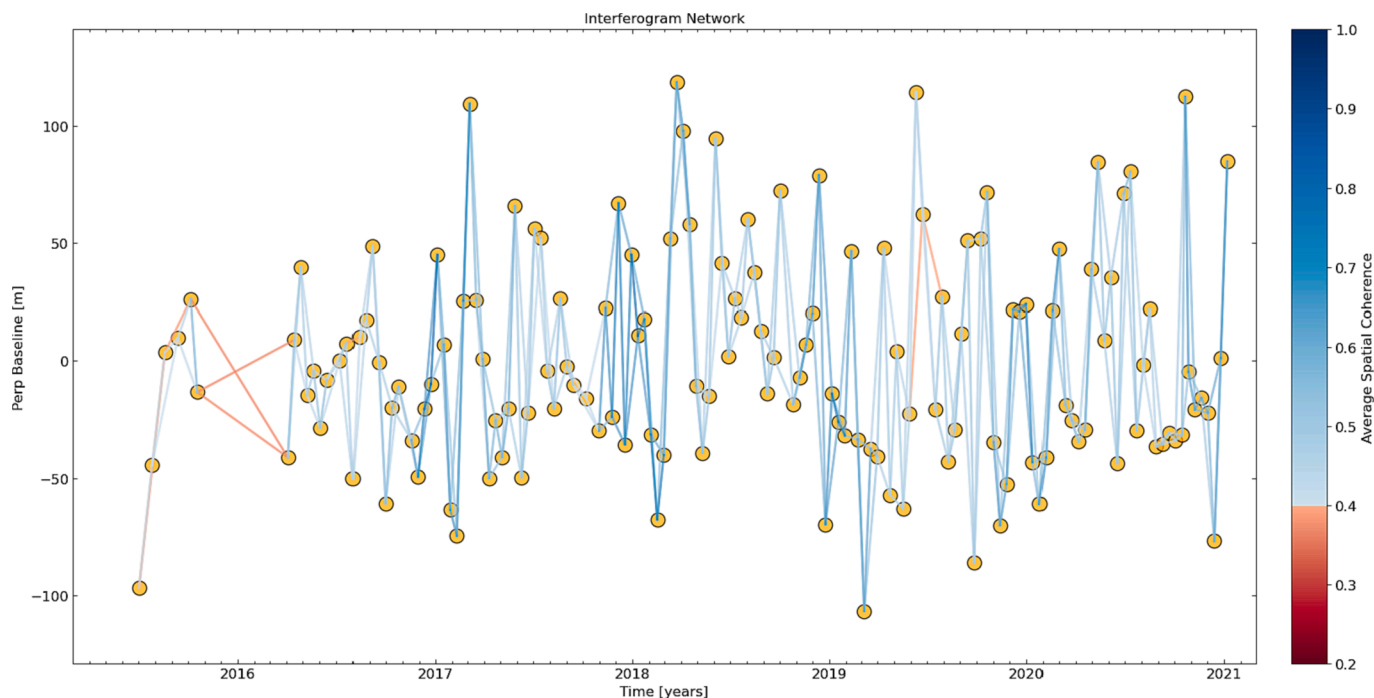
Fig. 3. Small baseline interferogram network. Yellow circles are the SLC images, the connections are the interferograms colour coded by the average spatial coherence. This network consists of 147 SLC images and 291 interferograms. (For interpretation of the references to colour in this figure legend, the reader is referred to the web version of this article.)

Network-flow Algorithm for Phase Unwrapping) proposed by Chen and Zebker (2002). This algorithm poses phase unwrapping as a maximum a posteriori probability estimation problem in order to compute the most likely unwrapped solution given the observable input data.

For the time series development, we processed the interferogram stack using the Miami INsar Time-series software in PYthon (MintPy) (Yunjun et al., 2019). The Small BASeline (SBAS) interferogram network is shown in Fig. 3. We used the SRTM 30 m digital elevation model (Farr et al., 2007) to estimate and correct the topographic error, and used ERA5 reanalysis weather model data to correct for atmospheric errors according to the method of Jolivet et al. (2014). All displacements were referred to the reference point located at 20.946 latitude and 105.742 longitude, which has relatively little displacement over time (i.e. it is stable) and with a temporal coherence of 0.995. Additionally, we removed a bilinear ramp from each interferogram to reduce any remaining long wavelength trends. We detect and correct unwrapping errors in the interferograms using the phase closure functionality in MintPy (Yunjun et al., 2019). The coherence pattern for each interferogram can vary depending on the difference between neighbouring acquisitions. MintPy allows pixels to drop in and out of coherence in the time series. However, we set an overall temporal coherence threshold of 0.7 to ensure we only include pixels in that remain coherent most of the time during the observation window (July 2015 to January 2021).

3.2. PCA and clustering

To facilitate the interpretation work on such a large dataset, we combined Principal Component Analysis (PCA) and an unsupervised cluster analysis, k-means, in order to characterise temporally and spatially changing deformation patterns without a-priori constraints.

For the PCA analysis, the time series of deformation obtained from the processing described in Section 3.1 has been standardised so that each time series has a zero mean and unit variance (Novellino et al., 2019; Festa et al., 2023). PCA is a signal processing method that, when applied to InSAR time series, aims to reduce dimensionality by aggregating random and intercorrelated time-dependent variables as a linear combination of statistically uncorrelated spatial components, also known as Principal Components or eigenvectors (Chaussard et al., 2014). The PCs can be used to reduce the effective number of dimensions in a data set while preserving its characteristics. Indeed, the PCs are ordered by percentage of variance explained and because the first PCs (or eigenvectors) contain the majority of the variance of the data, by discarding the later components, a large proportion of the variance of the data can be expressed in relatively few dimensions (Ebmeier, 2016). For InSAR, retrieving PCs, means identifying the main patterns of motions within the observed signals. We used the variance explained from the PCs result to constraint the number of groups to be selected in the cluster analysis. Usually, the highest change in the variance (also known as elbow point) distribution of the PCs provides an indication of when further components are no longer significant because they do not significantly affect the variability of data.

Clustering is an unsupervised machine learning technique where an algorithm groups similar data points starting from a collection of unlabelled data (Hubert and Arabie, 1985; Rygus et al., 2023).In the case of the K-means algorithm, samples are clustered in n groups of equal variance, minimising a criterion known as the inertia or within-cluster sum-of-squares, the latter measures the deviation of data points away from the mean value. This algorithm requires the number of clusters, n, to be specified. In this study, n has been selected based on the results of the PCA analysis. K-means scales well to large numbers of samples and has been already used to analysed InSAR time series (Festa et al., 2023).

4. Results

4.1. InSAR-derived observations of subsidence patterns in Hanoi

InSAR results cover an area of 16,400 km^2, including approximately 8 million measurement points with a temporal coherence > 0.7. The average velocity of each measurement point is computed by the linear fit through the time series displacements. These show localised maximum displacement rates up to -15 cm/yr (Fig. 4). Such velocities are similar to those observed for the period 2015–2018 by Nguyen et al. (2022) who validated against GNSS, results presented here show how ground deformation, compared to the previous decade (Dang et al., 2014), is now concentrated in the outskirts of the city centre.

Within this study we primarily focus on the Hanoi City, however, the InSAR results were processed for the wider Hanoi Metropolitan Area. To aid the interpretation of the InSAR data and help make the link to causal factors, rough polygons were drawn around areas showing the largest motions on the Sentinel-1 average velocity data (purple polygons on Fig. 4) and associated to cluster #2 and #3 (Fig. 5). These interpreted areas of motion range in size from small areas (<0.04 km^2) of discreet rapid motion to large polygons ($\sim$1400 km^2) outlining broad areas of motion.

In the authors' experience the large polygons following the major rivers in Fig. 4 outline areas of motion that likely result from the natural compaction of the recent alluvial sediments. Areas of relatively rapid motion to the south and west of central Hanoi (A, B and C in Fig. 4) form the focus of this paper.

To run the PCA, we must normalise the InSAR dataset so that all features are at the same scale and within the same range. This step is important since PCA is a variance-based approach that projects original data onto different directions maximising the variance. Usually, normalisation is done so that all features are at the same scale.

The first seven PCs together explain $\sim$90 % of the total variance of the InSAR data, indicating that only these PCs are sufficient to represent the variability of the InSAR timeseries. By doing so we are able to retain enough information from the data to fully characterised the different types of movements we would expect in Hanoi (Fig. 5). Based on the number of dominant PCs, we have therefore set to seven the number of groups in the k-mean cluster analysis (Fig. 5).

Despite the different rates seen within the 7 clusters, there are similarities where the same feature is observed in each cluster (e.g., peaks observed in May 2015, May 2019 and July 2020), these are probably connected to atmospheric disturbances in the original SAR images which generated phase jumps in the interferograms. Cluster #1 and #4 can be considered to represent stable areas and amount to $\sim$57 % of the total number of targets, the remaining clusters show long-term linear subsidence with different rates of displacement. Cluster #1 and #4 correspond to the stable central part of Hanoi while cluster #2, the cluster with the highest subsidence rate, is always surrounded by cluster #3, the cluster with the second highest subsidence rate, which in turn is surrounded by cluster #5, the cluster with the third highest subsidence rate a clue that they correspond to different sectors of a subsidence bowl (Fig. 5).

The SBAS results from 2015 to 2021 show the centre of Hanoi to be stable during this time period (Fig. 6a), spatially, subsidence is evident to the south, south-west and west of the city (Fig. 6a) in the Ha Dong, Hoai Duc and Dan Phuong districts. Subsidence rates are faster than the ones measured with other SAR sensors and InSAR techniques for the period 2007–2018 (Dang et al., 2014; Nguyen et al., 2022). Additionally, during the 2007–2011 period covered by the ALOS data used by Dang et al. (2014), the subsidence to the south of the city in Ha Dong was much closer to the city centre (see relative position of the black box in Fig. 6); it appears that this subsidence has migrated southwards during the 2015 to 2021 period and its magnitude almost doubled. Also, the subsidence observed in the sentinel data in Hoai Duc to the west of the centre does not have the same size or magnitude in the ALOS data.
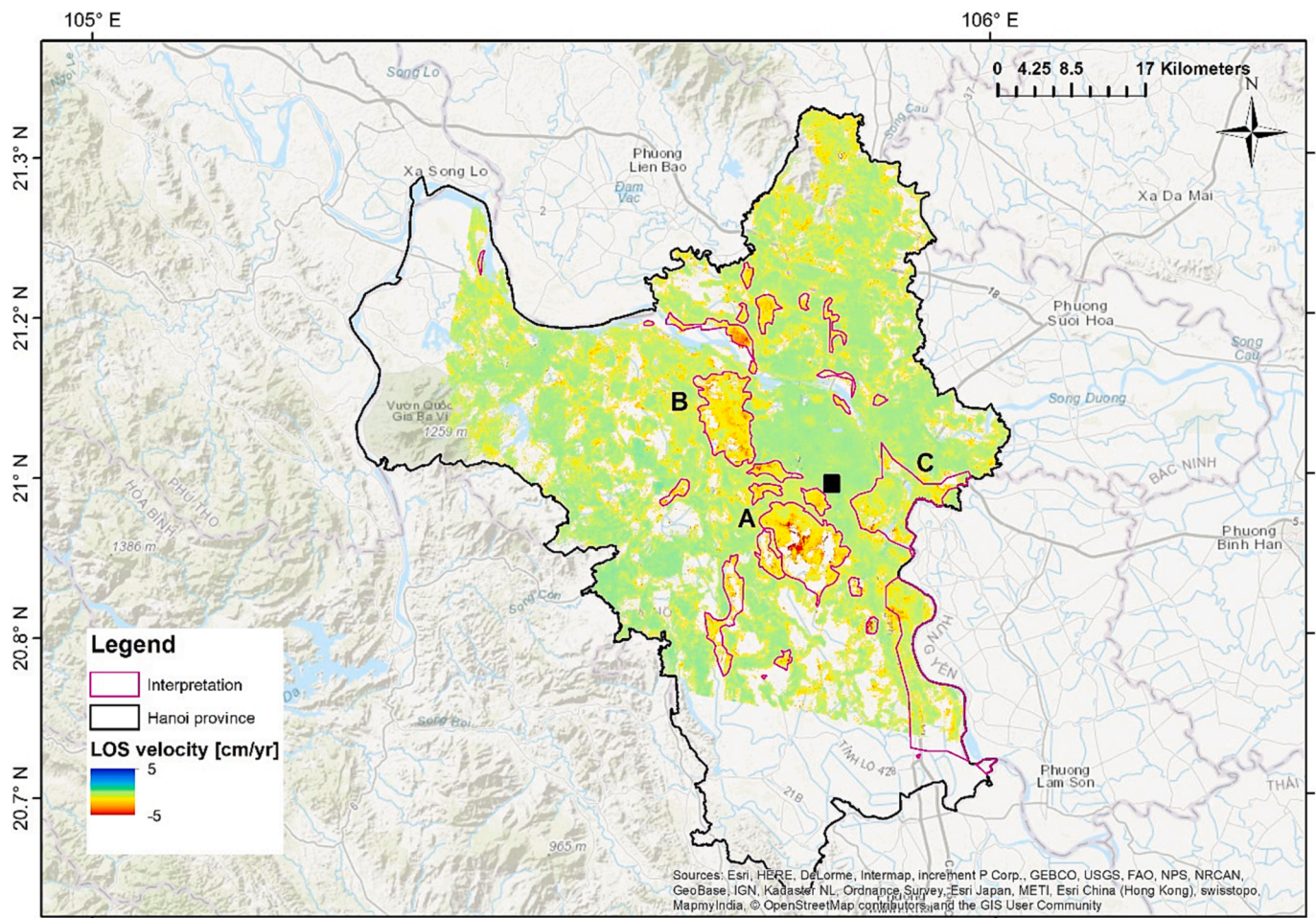
Fig. 4. Sentinel 1 derived InSAR data for Hanoi. Average velocity data displayed with interpreted areas of motion overlaid as purple polygons. Labels show location of other figures and study sites referred to in this paper, black square shows the location of the reference point. (For interpretation of the references to colour in this figure legend, the reader is referred to the web version of this article.)

Dang et al (2014) propose that the subsidence observed in 2007 to 2011 relates to ground water abstraction from wells Q65, Q64 and Q69 (Fig. 6). We observe, in the Sentinel-1 data, that the area around Q64 is now stable, the subsidence rate around the location of Q65 has decreased and that the whilst we still opbserve subsidence in the vacinity of Q69 in the sentinel and ALOS data, there is now a significant area of subsidence to the south east of Q69 which was not present in the ALSO data (Fig. 6a).

A comparison of the Sentinel-1 InSAR time series of the measurement points showing the most rapid motion (black star in Fig. 6a) with the groundwater levels in borehole Q69 (the closest borehole to the most rapid motions) reveals that the InSAR displacements do not directly follow the ground water abstraction curve as is typically observed when groundwater abstraction is the sole the mechanism responsible for ground motion (e.g. Herrera et al., 2009; Herra et al., 2010; Béjar-Pizarro et al., 2017). In the Q69 borehole we observe an overall low-erering of groundwater levels for the 2015–2019 period (Fig. 7), this average trend is reflected by the average trend of the InSAR time series. However, there are also other major changes in the groundwater levels which are not reflected in the InSAR time series: during 2016 the groundwater level fell by 10 m and then during 2017 the level rose by 8 m before continuing to rise more gradually. The Sentinel-1 InSAR time series reveals linear subsidence during this period period, and does not reflect the rapid lowering and subsequent rise of groundwater levels. Whilst it is true that there is a time lag between groundwater level changes (Bateson et al., 2009) and the response of the ground surface if groundwater change was the only factor causing the ground motion, we

would expect the InSAR time series to reflect these major changes in groundwater level more closely.

Nguyen et al. (2022), suggest four zones based on their comparison of Hanoi subsidence to groundwater change deformation modelling results:

- Zone a: severe subsidence with major groundwater level change.
- Zone b: substantial subsidence with minor groundwater level change.
- Zone c: minor subsidence with sustantial groundwater level change.
- Zone d: minor subsidence with minor groundwater level change.

They therefore find a correlation between groundwater level change and subsidence in zones a and d, however for zones b and c there is situation where the groundwater level change does not directly relate to observed rates of subsidence as observed in Nguyen et al. (2022). We suggest that there maybe a contribution to the subsidence rates in such areas from the loading of the ground during urban development.

4.2. Engineering geological properties and comparison to InSAR results

From the 3D geological model introduced in Section 2, a discrete smooth interpolation method has been used to extract the proportion of clay, fine sand and coarse sand material in the deposits (Fig. 8). A larger proportion of clay (50–60 % within the Quaternary sediments) is found to the south and west of Hanoi centre, whereas fine and coarse sand dominates in the northern, central, and southern parts of the Hanoi
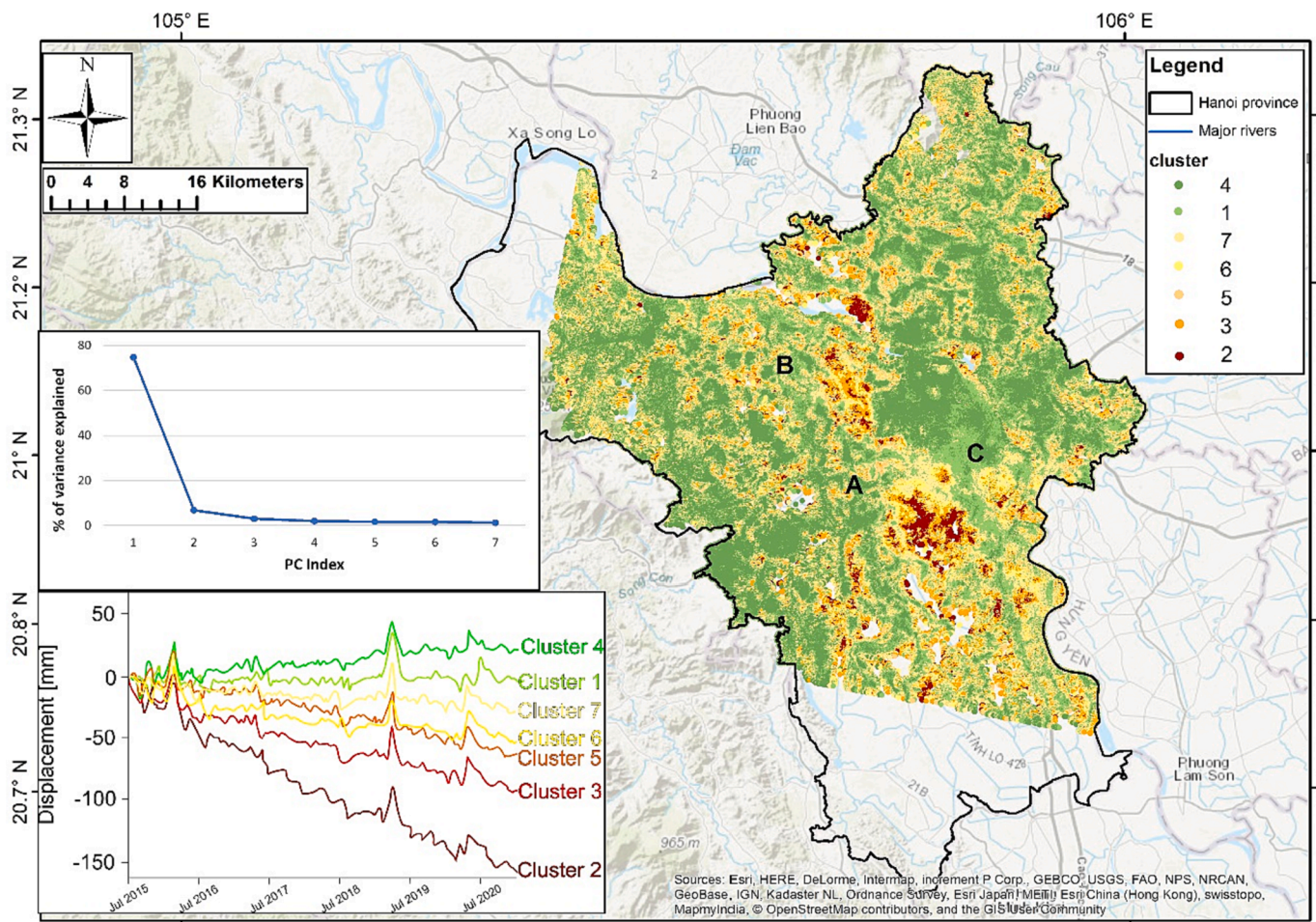
Fig. 5. Spatial distribution of the seven clusters within the Hanoi *Metropolitan Area. (inset left): Scree plot of the percentage of variance explained by each PC. (inset right) K-means clustering for seven groups. For each cluster, the median value (red solid line) is represented.* (For interpretation of the references to colour in this figure legend, the reader is referred to the web version of this article.)

Metropolitan Area.

It is evident from the distribution of materials derived from the 3D model that areas richer in clay correspond spatially with areas of cluster #2 and #3, namely the group of pixels with the fastest average subsidence rates (Fig. 8). The area with highest proportion of clay is in the Ha Dong area, in close proximity to the InSAR measurements with the most rapid motion (Fig. 6a). It is frustrating that the boreholes, from which the 3D model was constructed, do not extend fully into Ha Dong and therefore the information on material proportion does not cover the entire Ha Dong area. However, the information given does imply that the high clay proportion would extend southwards. The centre of Hanoi, which is now stable (Fig. 6a) has a higher proportion of sand than clay.

4.3. Urban development and subsidence

At the end of the 1980s the government subsidised housing scheme ended leading to increased private house construction with over 100 new residential zones developed (Dang et al., 2014). From 2003 there has been almost a 60 % increase in the area of artificial surfaces in Hanoi (Novellino et al., 2021), with the construction of large residential and commercial assets within the districts of Thuong Tin (~34,000 units) and Chuong My (~28,000 units) in the south and west part of the city centre, respectively (Bide et al., 2023).

The areas of fastest motion, as seen in the Sentinel-1 data, are found in Ha Dong to the south of Hanoi centre in polygon A in Fig. 4. Average rates of motion here are up to 9 cm of subsidence per year, it is evident from the cluster analysis that this subsidence takes the form of a bowl

(Fig. 5). The area in question is 1 km south-east of Phu Luong Ward, it is shown by the black star in Fig. 6a and in more detail in Fig. 9.

The InSAR time series shows initial stability followed by subsidence in early 2016, the rate of subsidence then declines; although the area is still subsiding in 2021 the rate is lower than in 2017. Historical imagery allows the ground conditions to be assessed for different periods of the InSAR time series (Fig. 10). We observe the reclamation of the land from agricultural areas to areas suitable for construction. The development process starts in 2016, the ground is loaded with aggregate, and we observe the onset of subsidence which continues to the end of 2016. The aggregate is initially emplaced along 'roadways' with the 'ponds' between the roads subsequently infilled. In this case the 'ponds' were infilled in early 2017, which corresponds with an increase in the subsidence rate (yellow arrow) throughout 2017. The subsidence rate starts to decline from 2018 onwards as the added material is vegetated (3/2018 - Fig. 10) and buildings are constructed (5/2020 - Fig. 10).

In Ha Dong we also observe new development polygons containing large buildings (Fig. 11, for location see Fig. 9) where the subsidence stops abruptly, initially it was thought that compaction may have ceased under these structures, however these structures are likely to be founded on deep foundations stretching to the Neogene sediments at a depth of 50–70 m (Dang et al., 2014). It is therefore possible that the initial subsidence (starting in 2016) is due to loading of the land by aggregate. However, once the tall and well-founded buildings are constructed (2018), the InSAR signal (average in an SBAS resolution cell) stabilises since it is dominated by the signal from the new buildings. The time series reflects this as a period of initial rapid subsidence followed by
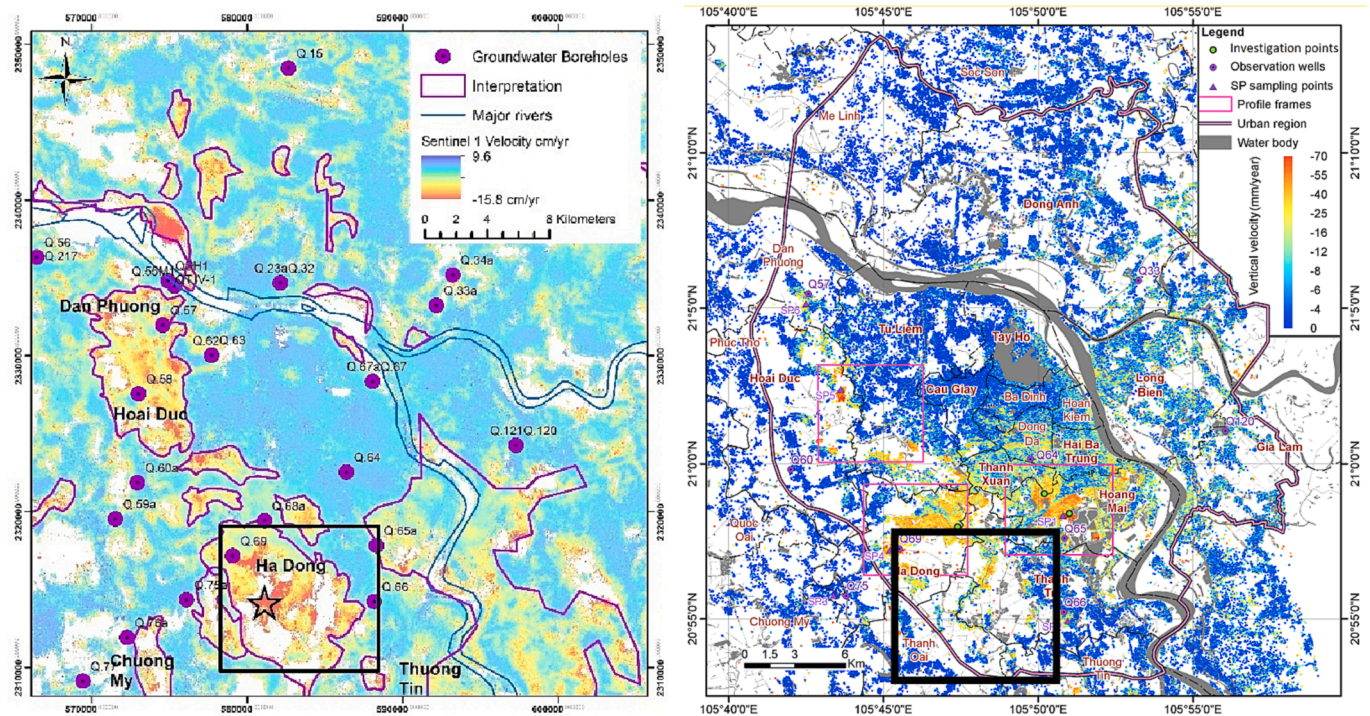
Fig. 6. A. sentinel 1 2015–2021 derived InSAR average velocities, b. ALOS InSAR 2007–2011 average velocities (modified from Dang et al., 2014). "World Imagery". Copyright © Esri. All rights reserved.
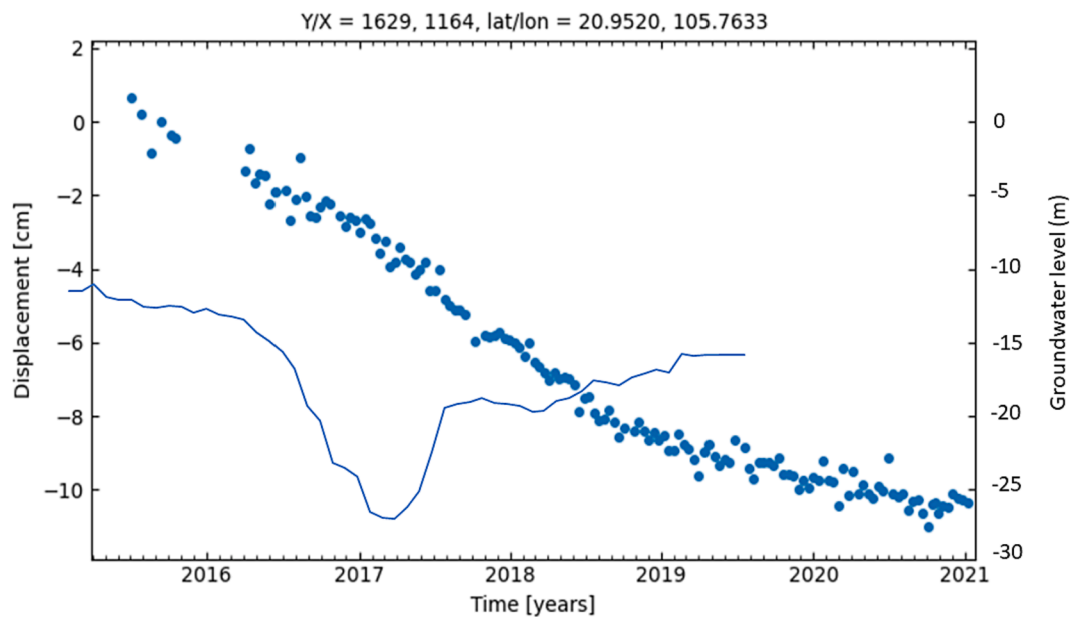

Fig. 7. Groundwater level change (solid blue line) at the Q69 borehole compared to the InSAR time series(blue points) for measurements points showing the most rapid motion during the 2015–2021 period, (black star in Fig. 6a). (For interpretation of the references to colour in this figure legend, the reader is referred to the web version of this article.)

stabilisation of the ground deformation.

4.4. Deriving subsidence rates following ground loading

Using the information on the age of development gained from the historical imagery available on Google Earth and the corresponding InSAR time series velocities within the polygons, we can derive the subsidence for each year following initial loading of the ground. However, we can only measure subsidence from the beginning of the InSAR

data (January 2015). So, if loading began in 2014 we will begin to measure the subsidence pattern a year into the process.

The derived yearly subsidence rates for area A, which corresponds to the fastest subsidence rates in the Ha Dong area, (Fig. 4, Fig. 10) are given in Table 2, which shows the subsidence for each year following the loading of the ground during urban development in Hanoi. In general the rate is faster immediately following the loading and then declines in subsequent years. In this case, subsidence in the first year is less than in the second, this is possibly due to the gap in the time series in early 2016

Fig. 8. a (top left). Sentinel 1 InSAR clusters. B (top right). Clay proportion extracted from the geological model. C (bottom left) Fine sand proportion. D (bottom right). Coarse sand proportion.
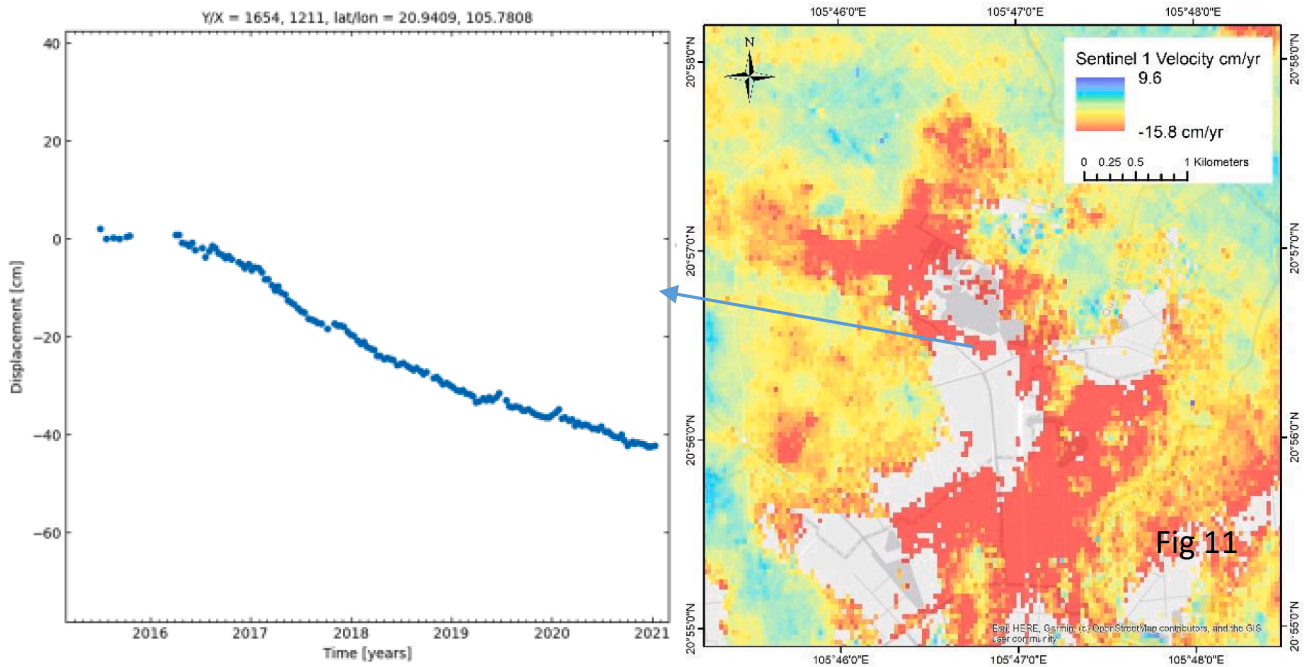
Fig. 9. The area of rapid motion to the south east of Phu Luong Ward, right: average velocity, left: InSAR time series, which has been extracted for a representative SBAS pixel as indicated by the arrow.
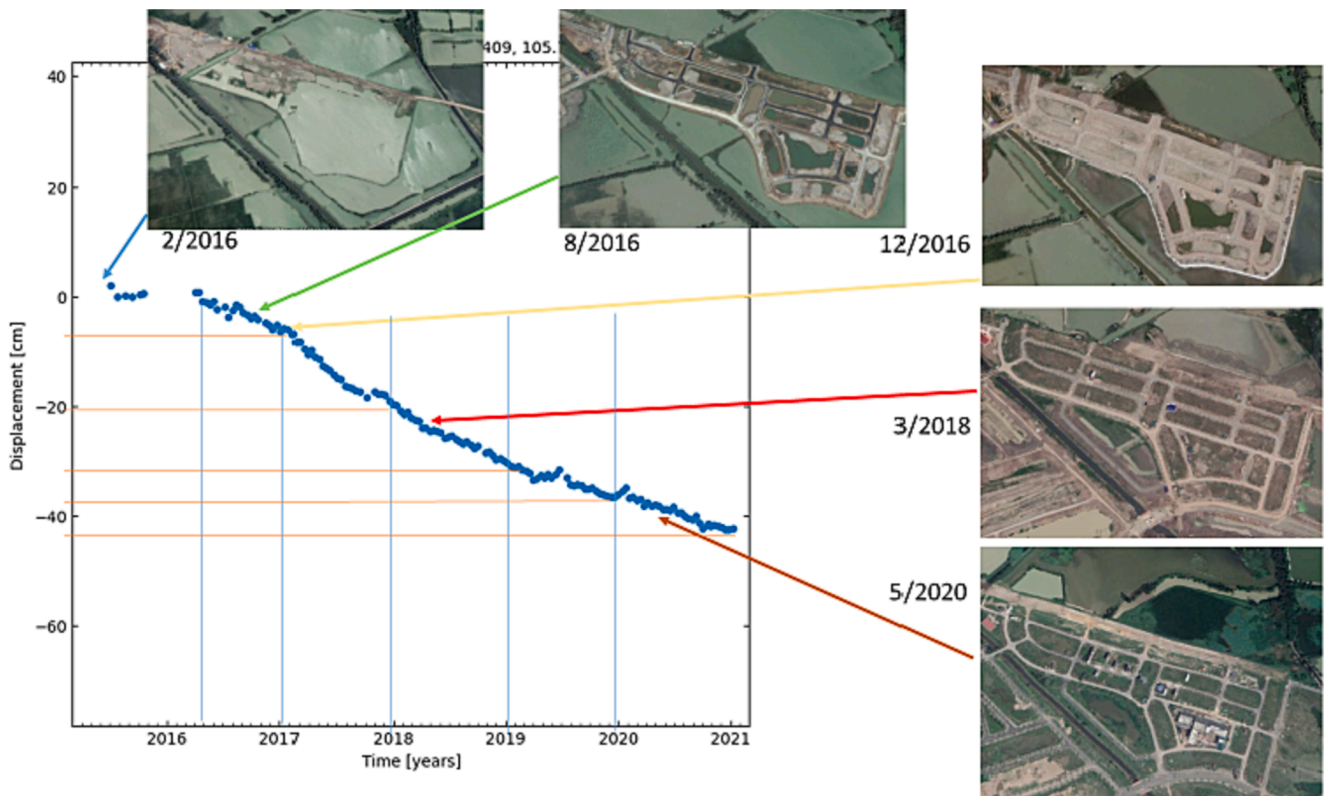

Fig. 10. Area A in Ha Dong, representative InSAR time series for an area of rapid motion to the south east of Phu Luong Ward has been plotted for a single SBAS pixel as indicated by the arrow in Fig. 9. Imagery, with accompanying dates, shows the progressive infill and loading of this previously flooded area with aggregate. Image © Airbus 2023, Image © Maxar Technologies 2023 (accessed via Google Earth).

when coherence was lost due to water coverage and loading continued into 2017, which would increase the subsidence in subsequent years.

Recognising that it might be possible to extract rates of subsidence relating to the loading of the ground in other areas of Hanoi and using cluster #2 and #3 as a spatial constraint, we then analysed Google Earth optical imagery for the areas of fastest motion in Ha Dong, Hoai Duc and
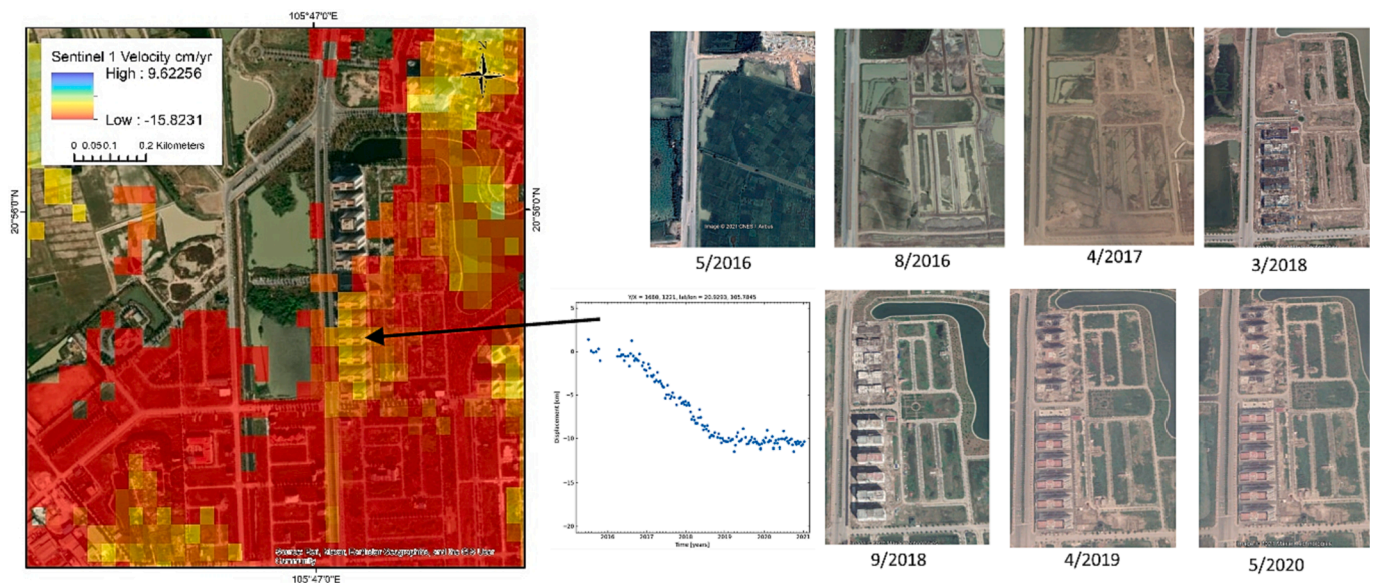
Fig. 11. Area of development where the land was initially loaded by aggregate leading to subsidence in 2016 to early 2018. Once buildings with piled foundations are constructed, we see a stabilisation in the time series. Due to the nature of the SBAS InSAR processing, where interferometric coherence is calculated between adjacent acquisitions which have short temporal baselines (12–24 days in our baseline network), it is possible to retain coherence when dramatic changes in landcover occur over time if the change is incremental (such as construction activity at a new building site). InSAR timeseries is extracted for a single SBAS pixel as indicated by the arrow. Image © Airbus 2023, Image © Maxar Technologies 2023 (accessed via Google Earth).

Table 2
Derived yearly subsidence rates for Area A in Ha Dong, to the south east of Phu Luong Ward.

Location	Rate year 1 (following loading of ground) (2016)	Rate year 2 (2017)	Rate year 3 (2018)	Rate year 4 (2019)	Rate year 5 (2020)
Area A, site 1	6 cm/yr.	16 cm/yr.	11 cm/yr.	5.5 cm/yr.	5 cm/yr.

Dan Phuong (areas A, B and C in Fig. 4) where many areas of land have been developed since 2008. From the high-resolution optical satellite images, we digitised polygons around the areas of development and each polygon was attributed with the month and year of first development activity (Fig. 12).

Within Fig. 12, two observations are important: (1) the co-incidence of areas of development with areas of subsidence; almost all areas of subsidence identified between 2015 and 2021 correspond with areas developed within the last 12 years. (2) Areas developed more recently show faster rates of subsidence in the 2015–2021 InSAR, this ties with the observations initially made at Ha Dong, where we observe a decline in subsidence rates as time passes from the onset of development.

In order to derive more representative rates related to development we focused our further study on development in Ha Dong; the area with the fastest average velocities. InSAR time series were used in conjunction with the historical satellite imagery to derive a rate of motion for each year following the development. For each of the 40 polygons
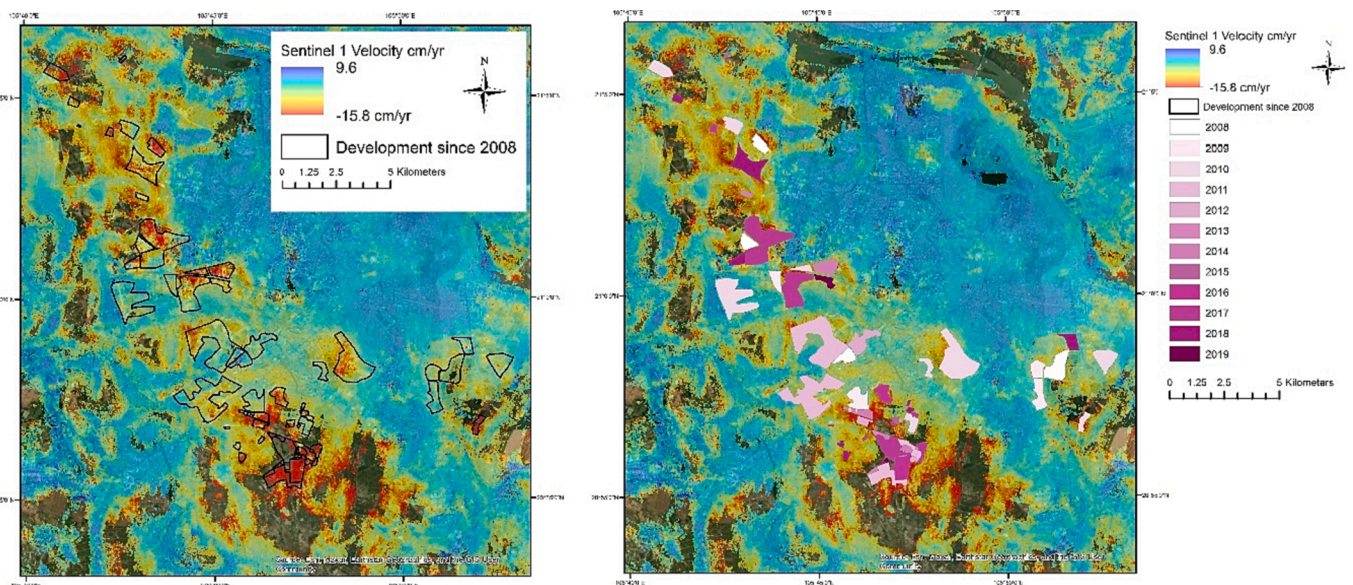

Fig. 12. Left: Areas of new development 2008–2021 as interpreted from multi-temporal satellite imagery overlain on the Sentinel 1 InSAR average velocity. Right: development polygons coloured by year of first ground loading. Image © Airbus 2023, Image © Maxar Technologies 2023 (accessed via Google Earth).

identified we calculate the rates of motion for each complete calendar year following the initial loading. Fig. 13 shows detail for a subset of the polygons analysed.

Calculated rates were recorded for each polygon individually and then aggregated and averaged into a subsidence rate for each year following the loading of the ground during construction which corresponds to year 0. The results are given in Table 2.

Since the InSAR data covers the 2015 to 2021 period and the developed polygons cover the 2008–2020 period we are able to study the entire consolidation period; i.e. if an area was developed in 2008 the InSAR time series captures the latter part of the consolidation phase (2015 corresponds to 8 years after the loading in 2008), the period where the subsidence is declining or stabilising. Whereas for an area developed in 2018 the time series captures the more rapid motion at the start of the consolidation process (Fig. 14).

Table 3 and Fig. 14 show that there is a correlation between subsidence velocities and construction years in the newly developed areas and that a consolidation curve can be extracted from these observations. It is apparent from the plots that there are some outliers; for example, the line "A", which corresponds to an area that was initially loaded in 2012. The rates for this area appear to be higher than other areas with a similar loading history. The same is true for the line "B" in Fig. 14. This corresponds to an area first loaded in 2016 and the initial rates of motion are 5 cm higher than all other areas, this area has the highest subsidence rates in Hanoi. It is possible that these outliers represent errors in the

identification of the first year of loading, but also possible that another mechanism, such as groundwater abstraction, is adding to the subsidence rate in these locations. Removal of such outliers allows for an average rate of subsidence following the loading of the ground during construction to be derived as given in Fig. 15.

5. Discussion

The pattern of subsidence in Hanoi over the 2015–2021 period offers interesting insights into the geological and anthropological processes taking place. The centre of Hanoi is stable, this is likely a reflection of its age and therefore the fact that all consolidation of the underlying sediments has taken place. To the south and west of Hanoi centre areas of rapid subsidence exist in the data processed between 2015 and 2021. Similarities and differences with earlier InSAR data highlights the progression of subsidence phenomena as areas stabilise and the subsidence appears to migrate in response to the governing processes. In this case the apparent migration of the subsidence relates to the shift in areas of development away from the centre of Hanoi. To the south of Hanoi centre small areas of high subsidence rates correlate with areas of new industrial development, this raised the question of if the subsidence was due to the development of the industry or possible groundwater abstraction to be used in said industry. Answering this question is outside of the scope of the current study, partially due to a lack of groundwater abstraction data for such areas and partially due to
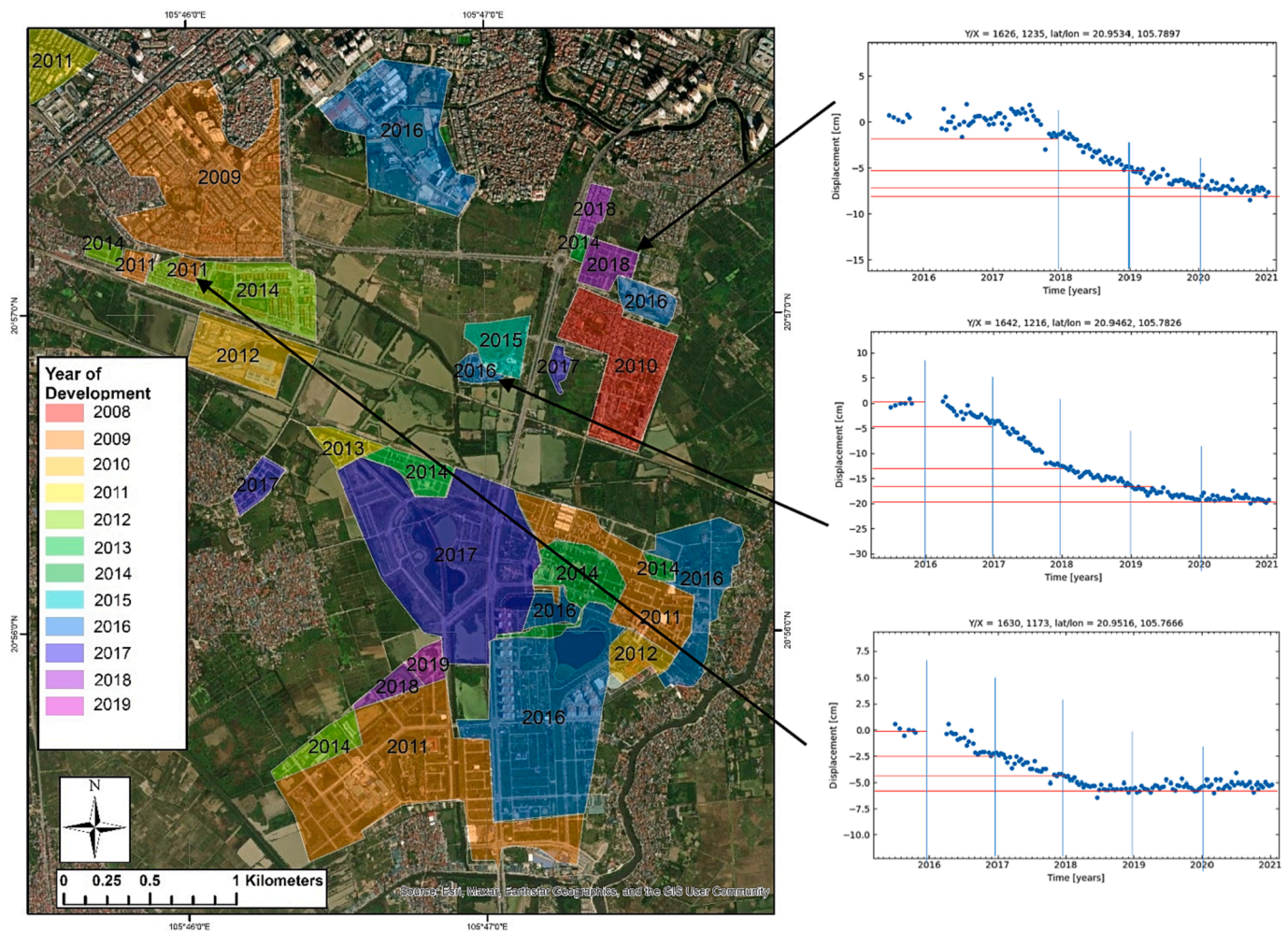

Fig. 13. Detailed interpreted development polygons for Ha Dong, each polygon is labelled with the month and year of the imagery on which development was first observed. Three selected time series plots are shown to illustrate the subsidence rates with time after loading. Top was loaded in 2018, middle in 2016 and bottom in 2014. Image © Airbus 2023, Image © Maxar Technologies 2023 (accessed via Google Earth).
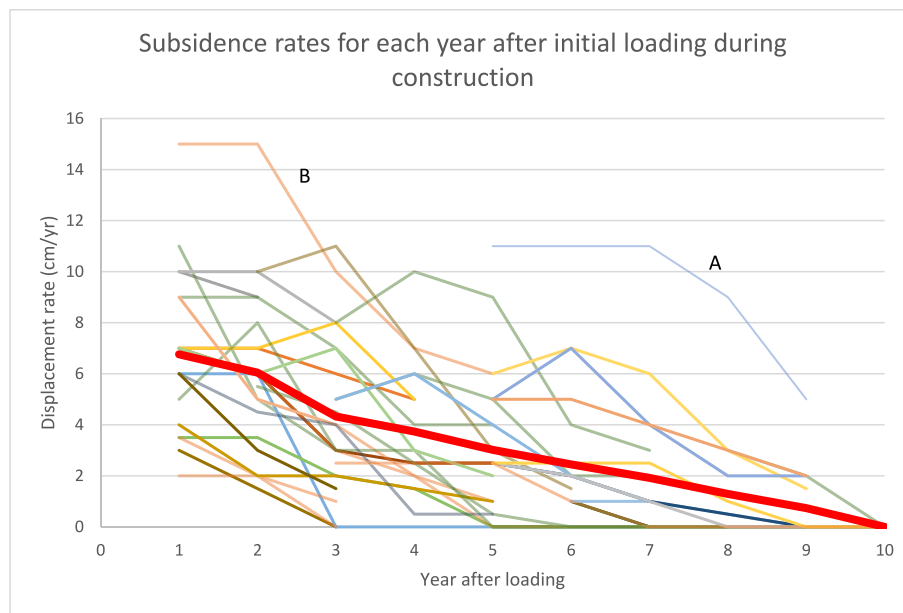
Fig. 14. Graphical plot of data in Table 2; each line represents a single area of development for which rates of subsidence have been derived. The lines show the amount of subsidence for each year following the loading of the ground during construction for each polygon drawn in Fig. 15. Thick red line shows the average of all observations. (For interpretation of the references to colour in this figure legend, the reader is referred to the web version of this article.)

incomplete InSAR coverage.

However, closer to the centre of Hanoi, in Ha Dong, Hoai Duc and Dan Phuong, a very clear relationship exists between areas that have undergone substantial development since 2008, as identified on time series of optical satellite imagery, and rapid rates of subsidence between 2015 and 2021. These areas are locations where other authors have noted a disparity between rapid rates of subsidence and low rates of ground water abstraction.

We have been able to demonstrate through the integrated interpretation of time series of high-resolution optical satellite imagery and Sentinel 1 derived InSAR measurements that a clear spatial and temporal association exists between areas of new development around the outskirts of Hanoi and rapid rates of subsidence. InSAR results at higher spatial resolution have been used in studies of small developments to characterise the consolidation processes in relationship with the local stratigraphic setting and the geotechnical properties of the subsoil (Bozzano et al., 2018). We found that in the case of the larger extent of urban development in Hanoi C-band InSAR has been sufficient for our analysis. In the case of our Ha Dong study area, to the south of Hanoi centre, we observe an average rate of nearly 7 cm during the first year following ground loading, this falls away in almost a linear fashion until the 10th year when the ground stabilises as consolidation stops. The relationship also allows an average total expected subsidence to be calculated, this is on average 31 cm.

Within the Ha Dong study site there is a variation in subsidence rates of over 10 cm for the first year following loading, the variation decreases the longer that the loading is taking place. It is possible that such variation may relate to differences in the local sedimentary succession, for example areas with more gravel will undergo less consolidation than areas with a higher proportion of clay. To test this hypothesis would require a greater number of interpreted boreholes in the Ha Dong area (currently boreholes are limited to the very north of this area). Observed variations in subsidence rate may also relate to the thickness of the aggregate added to the land surface in different areas, it is also likely that in some areas subsidence rates are a combination of ground loading and groundwater extraction.

The rapid development in the last 20 years relates to relaxing of the planning laws in Vietnam. It is interesting to observe that subsidence relates not to the timing of the construction of buildings but to the

loading of previously wet or flooded areas of land with aggregate. In fact, there are examples where the new buildings appear to stabilise the area as seen in the InSAR data. This is likely to be because the buildings are built on suitable pile foundations and therefore stable. Once built the radar backscatter signal from the stable buildings will dominate the InSAR measurement for the SBAS resolution cell, the ground around the building may still be subsiding but backscattered radar signals will not be as strong from such surfaces due to the nature of the surface. This relationship highlights possible hazards that might occur due to the differential motion of the stable buildings and ongoing subsidence of the surrounded land; subsurface services, such as gas, water and electric, are buried in the reclaimed land and then enter the building. At the point of entry differential subsidence between the made ground and piled building could lead to failure of the service, which at best would be expensive but in the case of a gas pipe could be dangerous.

The derived relationship has clear implications for the planning of development in low lying deltaic environments such as Hanoi, where thick successions of poorly consolidated recent sedimentary deposits form the basis for the urban environment. Such a situation exists in many low-lying deltaic environments currently undergoing rapid urbanisation and development. The relationship derived in this work has applications for the planning of such new developments; rates of expected subsidence can be factored into calculations to ensure safer developments as the hazard can be mitigated against. Analysis of more rapidly growing cities in similar geological environments will increase the statistical validity of the derived relationship as the sample size is increased.

6. Conclusions

We have demonstrated a clear relationship between the InSAR observed subsidence for six years in the vicinity of Hanoi and areas where the ground has been loaded during development over the last 13 years. Rates of motion following the loading of the ground have been calculated from the InSAR time series: the subsidence rate is highest in the first year, with nearly 7 cm/yr of subsidence, and the rate linearly declines to 0 cm/yr after 10 years.

Although subsidence is expected and planned for when loading and developing the ground, spaceborne InSAR offers the ability to remotely

Table 3

Derived yearly subsidence (in cm) for each polygon of development in the Ha Dong area (see Fig. 13). For each polygon (corresponding to each row) analysed, the year of first loading, as derived from the optical imagery, is given in the first column. Subsequent columns then give the subsidence value for each year following the initial loading. For example, if a polygon was first loaded in 2010 then subsidence measurements are possible from 2015 onwards; the year when the Sentinel 1 data acquisition started.

| Development polygon ID	Year of first loading	Subsidence, in cm, for each year following initial loading									
		Year 1	Year 2	Year 3	Year 4	Year 5	Year 6	Year 7	Year 8	Year 9	Year 10
1	2008								3	2	0
2	2010					0	0	0	0	0	0
3	2010						1	0	0	0	0
4	2010						1	1	0.5	0	0
5	2012					11	11	11	9	5	
6	2012					6	7	6	3	1.5	
7	2012					5	7	4	2	2	
8	2012					2.5	2	1	0.5	0	0
9	2012					5	5	4	3	2	
10	2012					2.5	2	1	0	0	0
11	2012					2.5	2.5	2.5	1	0	0
12	2014			4	2	0	0	0	0	0	0
13	2014			8	10	9	4	3			
14	2014			5	6	5	2	2			
15	2014			5	6	4	2	1			
16	2014			2.5	2.5	2.5	1	0	0	0	0
17	2015	6	6	3	2	1					
18	2015		5.5	4.5	2.5	0.5	0	0	0	0	0
19	2015		10	11	7	3	1.5				
20	2016	7	13	11	5	5					
21	2016	5									
22	2016	9	9	7	4	4					
23	2016	7	6	3	2.5	2.5					
24	2016	6	6	0	0	0	0	0	0	0	0
25	2016	15	15	10	7	6					
26	2016	7	7	8	5						
27	2016	3.5	3.5	2	1.5	0	0	0	0	0	0
28	2016	4	2	2	1.5	1					
29	2016	5	8	3	3	0	0	0	0	0	0
30	2016	7	6	7	3	2					
31	2016	6	4.5	4	0.5	0.5					
32	2017	7	7	6	5						
33	2017	10	10	8							
34	2018	11	5	3							
35	2018	3	1.5	0							
36	2018	2	2	0							
37	2018	3.5	2	1							
38	2018	9	5	4							
39	2018	6	3	1.5							
40	2019	10	9								
	Average	6.77	6.35	4.57	3.80	3.10	2.45	1.92	1.29	0.74	0.00
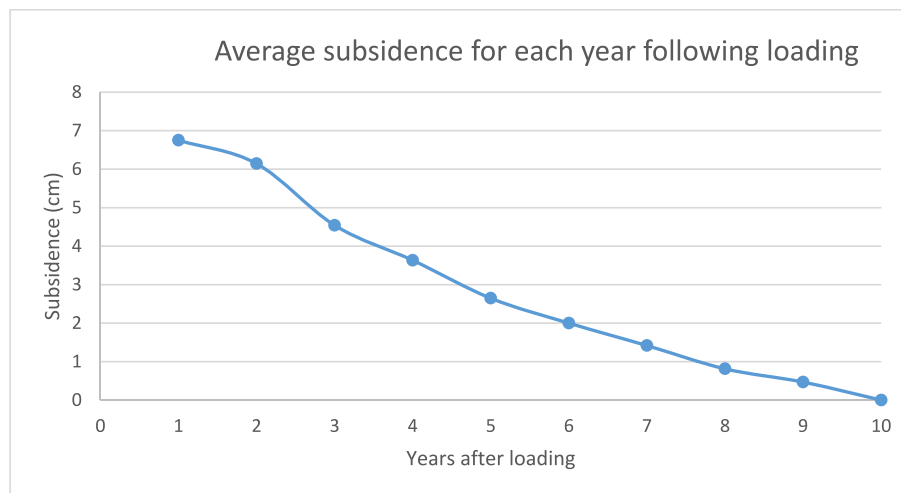
Fig. 15. Average rate of subsidence following loading during construction in Hanoi (outliers removed).

monitor actual rates over large areas.

The analysis provides valuable information on the general state of operation of new infrastructures and could be useful for planning maintenance and simplifying inspection operations. These results provide local authorities with an overview of the consolidation conditions at both large and small scale and offer a time- and cost-effective solution to identify anomalous areas and define intervention priorities.

Declaration of competing interest

The authors declare that they have no known competing financial interests or personal relationships that could have appeared to influence the work reported in this paper.

Data availability

The authors do not have permission to share data.

Acknowledgments

References

Arnhardt, R., Novellino, A., Hussain, E., Bateson, L., Newell, A. (2023). Land subsidence susceptibility mapping for Hanoi city, Vietnam. In *Submitted to proc of the tenth international symposium on land subsidence (TISOLS) 2023*.

Bateson, L.B., Barkwith, A.K.A.P., Hughes, A.G., Aldiss, D.T. (2009). Terrafirma : London H-3 Modelled Product : comparison of PS data with the results of a groundwater abstraction related subsidence model. Nottingham, UK, British Geological Survey, 43pp. (OR/09/032) (available at: https://nora.nerc.ac.uk/id/eprint/8581/).

Béjar-Pizarro, M., Ezquerro, P., Herrera, G., Tomás, R., Guardiola-Albert, C., Hernández, J.M.R., Merodo, J.A.F., Marchamalo, M., Martínez, R., 2017. Mapping groundwater level and aquifer storage variations from InSAR measurements in the Madrid aquifer, Central Spain. Journal of Hydrology 547, 678–689. https://doi.org/10.1016/j.jhydrol.2017.02.011.

Bide, T., Novellino, A., Petavratzi, E., Watson, S., 2023. A bottom-up building stock quantification methodology for construction minerals using Earth Observation. The case of Hanoi. Cleaner Environmental Systems 8, 100109. https://doi.org/10.1016/j.cesys.2023.100109.

Bozzano, F., Esposito, C., Mazzanti, P., Patti, M., Scancella, S., 2018. Imaging multi-age construction settlement behaviour by advanced SAR interferometry. Remote Sensing 10 (7), 1137. https://doi.org/10.3390/rs10071137.

Bui, L.K., Le, P.V., Dao, P.D., Long, N.Q., Pham, H.V., Tran, H.H., Xie, L., 2021. Recent land deformation detected by Sentinel-1A InSAR data (2016–2020) over Hanoi, Vietnam, and the relationship with groundwater level change. Giscience & Remote Sensing 58 (2), 161–179. https://doi.org/10.1080/15481603.2020.1868198.

Chaussard, E., Bürgmann, R., Shirzaei, M., Fielding, E.J., Baker, B., 2014. Predictability of hydraulic head changes and characterization of aquifer-system and fault properties from InSAR-derived ground deformation. Journal of Geophysical Research: Solid Earth 119 (8), 6572–6590. https://doi.org/10.1002/2014JB011266.

Chen, C.W., Zebker, H.A., 2002. Phase unwrapping for large SAR interferograms: Statistical segmentation and generalized network models. IEEE Transactions on Geoscience Remote Sensing 40, 1709–1719. https://doi.org/10.1109/TGRS.2002.802453.

Dang, V.K., Doubre, C., Weber, C., Gourmelen, N., Masson, F., 2014. Recent land subsidence caused by the rapid urban development in the Hanoi region (Vietnam) using ALOS InSAR data. Natural Hazards and Earth System Sciences 14 (3), 657–674. https://doi.org/10.5194/nhess-14-657-2014.

Ebmeier, S.K., 2016. Application of independent component analysis to multitemporal InSAR data with volcanic case studies. Journal of Geophysical Research: Solid Earth 121 (12), 8970–8986.

Farr, T.G., Rosen, P.A., Caro, E., Crippen, R., Duren, R., Hensley, S., Kobrick, M., Paller, M., Rodriguez, E., Roth, L., et al., 2007. The shuttle radar topography mission. Review Geophysics 45. https://doi.org/10.1002/2016JB013765.

Festa, D., Novellino, A., Hussain, H., Bateson, L., Casagli, N., Confuorto, L., Del Soldato, M., Raspini, F. (2023). Automatic detection of clusters of ground deformation from InSAR time series. *International Journal of Applied Earth Observation and Geoinformation, 118*, 103276. https://doi.org/10.1016/j.jag.2023.103276.

Gee, D., Bateson, L., Grebby, S., Novellino, A., Sowter, A., Wyatt, L., Marsh, S., Morgenstern, R., Athab, A., 2020. Modelling groundwater rebound in recently abandoned coalfields using DInSAR. Remote Sensing of Environment 249. https://doi.org/10.1016/j.rse.2020.112021.

GSOVa (2019). Statistics database—Data on population and employment. Available online: https://www.gso.gov.vn/en/homepage/ (last accessed: 30th December 2020).

GSOVb (2019). Statistical yearbook of Vietnam 2019: https://www.gso.gov.vn/wp-content/uploads/2020/09/Nien-giam-thong-ke-day-du-2019.pdf (last access: 4th March 2021).

Herrera, G., Fernández, J.A., Tomás, R., Cooksley, G., Mulas, J., 2009. Advanced interpretation of subsidence in Murcia (SE Spain) using A-DInSAR data–modelling and validation. Natural Hazards and Earth System Sciences 9 (3), 647–661. https://doi.org/10.1126/science.abb8549.

Herrera-García, G., Ezquerro, P., Tomás, R., Béjar-Pizarro, M., López-Vinielles, J., Rossi, M., Mateos, R.M., Carreón-Freyre, D., Lambert, J., Teatini, P., Cabral-Cano, E., 2021. Mapping the global threat of land subsidence. Science 371 (6524), 34–36.

Hubert, L., Arabie, P., 1985. Comparing partitions. Journal of Classification 2 (1), 193–218.

Vietnam Institute of Architecture, Urban and Rural Planning (VIAP) (2011). *Hanoi capital construction master plan to 2030 and vision to 2050, comprehensive report*. VIAP, Hanoi.

Jolivet, R., Agram, P.S., Lin, N.Y., Simons, M., Doin, M.P., Peltzer, G., Li, Z., 2014. Improving InSAR geodesy using global atmospheric models. Journal of Geophysics Research Solid Earth 119, 2324–2341. https://doi.org/10.1002/2013JB010588.

Kubota, T., Lee, H.S., Trihamdani, A.R., Phuong, T.T.T., Tanaka, T., Matsuo, K., 2017. Impacts of land use changes from the Hanoi Master Plan 2030 on urban heat islands: part 1. Cooling effects of proposed green strategies. Sustainable Cities and Society 32, 295–317. https://doi.org/10.1016/j.scs.2017.04.001.

Le, T.S., Chang, C.P., Nguyen, X.T., Yhokha, A., 2016. TerraSAR-X data for high-precision land subsidence monitoring: A case study in the historical centre of Hanoi, Vietnam. Remote Sensing 8 (4), 338. https://doi.org/10.3390/rs8040338.

Liou, Y.-A., Nguyen, K.-A., Ho, L.-T., 2021. Altering urban greenspace patterns and heat atreaa risk in Hanoi city during Master Plan 2030 implementation. Land Use Policy 105, 105405.

Nguyen, M., Lin, Y.N., Tran, Q.C., Ni, C.F., Chan, Y.C., Tseng, K.H., Chang, C.P., 2022. Assessment of long-term ground subsidence and groundwater depletion in Hanoi, Vietnam. Engineering Geology 299, 106555. https://doi.org/10.1016/j.enggeo.2022.106555.

Novellino, A., Brown, T.J., Bide, T., Thục Anh, N.T., Petavratzi, E., Kresse, C., 2021. Using satellite data to analyse raw material consumption in Hanoi, Vietnam. Remote Sensing 13 (3), 334. https://doi.org/10.3390/rs13030334.

Novellino, A., Terrington, R., Christodoulou, V., Smith, H., Bateson, L. (2019). Ground motion and stratum thickness comparison in Tower Hamlets, London. Nottingham, UK, British Geological Survey, 31pp. (OR/19/043). Available at: https://nora.nerc.ac.uk/id/eprint/525619/.

Peduto, D., Nicodemo, G., Maccabiani, J., Ferlisi, S., 2017. Multi-scale analysis of settlement-induced building damage using damage surveys and DInSAR data: A case study in The Netherlands. Engineering Geology 218, 117–133. https://doi.org/10.1016/j.enggeo.2016.12.018.

Phi, T.H., Strokova, L.A. (2015). Prediction maps of land subsidence caused by groundwater exploitation in Hanoi, Vietnam. *Resource – Efficient Technologies, 1*(2), 80–89.

Rosen, P.A., Gurrola, E., Sacco, G.F., Zebker, H. The InSAR Scientific Computing environment. In *Proceedings of the 9th european conference on synthetic aperture radar, EUSAR 2012*. Nuremberg, Germany, 23–26 April 2012 (pp. 730–733).

Rosen, P.A., Gurrola, E.M., Agram, P., Cohen, J., Lavalle, M., Riel, B.V., Fattahi, H., Bekaert, D.P.S., Aivazis, M.A., Simons, M., et al. (2021). The interferometric synthetic aperture radar scientific computing environment (ISCE2), v2.3.3. Available online: https://github.com/isce-framework/isce2 (accessed on 1 June 2020).

Rygus, M., Novellino, A., Hussain, E., Syafiudin, F., Andreas, H., Meisina, C., 2023. A clustering approach for the analysis of InSAR time series: Application to the Bandung Basin (Indonesia). Remote Sensing 15 (15), 3776.

Strozzi, T., Delaloye, R., Poffet, D., Hansmann, J., Loew, S., 2011. Surface subsidence and uplift above a headracetunnel in metamorphic basement rocks of the Swiss Alps as detected by satellite SAR interferometry. Remote Sensing Environment 115, 1353–1360. https://doi.org/10.1016/j.rse.2011.02.001.

Tosi, L., Teatini, P., Strozzi, T., 2013. Natural versus anthropogenic subsidence of Venice. Science Reports 3, 2710. https://doi.org/10.1038/srep02710.

Trafford, J.M., Lawrence, A.R., Macdonald, D.M.J., Nguyen, V.D., Tran, D.N., Nguyen, T.H. (1996). The effect of urbanisation on the groundwater quality beneath the city of Hanoi, Vietnam. BGS technical report WC/96/22.

United Nations, Department of Economic and Social Affairs, Population Division (2019). World Urbanization Prospects 2018: Highlights (ST/ESA/SER.A/421).

Vu, X.B., Nghiem, S., 2016. Analysis of GDP trends and inequalities in Vietnam's provinces and groups of provinces. Asian Journal of Empirical Research 6, 167–186.

Wakode, H.B., Baier, K., Jha, R., Azzam, R., 2018. Impact of urbanization on groundwater recharge and urban water balance for the city of Hyderabad, India.

International Soil and Water Conservation Research 6 (1), 51–62. https://doi.org/10.1016/j.iswcr.2017.10.003.

Yunjun, Z., Fattahi, H., Amelung, F., 2019. Small baseline InSAR time series analysis: Unwrapping error correction and noise reduction. Computational Geosciences 133, 104331. https://doi.org/10.1016/j.cageo.2019.104331.